Earth's Future

RESEARCH ARTICLE
10.1029/2024EF005166

Projected Changes to Characteristics of El Niño-Southern Oscillation, Indian Ocean Dipole, and Southern Annular Mode Events in the CMIP6 Models

C. T. Y. Chung[1], S. B. Power[2,3,4], G. Boschat[1], Z. E. Gillett[5], and S. Narsey[1]

[1]Bureau of Meteorology, Docklands, VIC, Australia, [2]ARC Centre of Excellence for Climate Extremes, School of Earth, Atmosphere and Environment, Monash University, Clayton, VIC, Australia, [3]Centre for Applied Climate Sciences, University of Southern Queensland, Toowoomba, QLD, Australia, [4]Climate Services International, Oakleigh, VIC, Australia, [5]ARC Centre of Excellence for Climate Extremes, Climate Change Research Centre, University of New South Wales, Sydney, NSW, Australia

Key Points:

- Using all available models and ensemble members, the latest generation of climate models project an overall increase to the frequency of El Niño-Southern Oscillation (ENSO) events but a weakening and decrease in Indian Ocean Dipole (IOD) events in the late 21st century. The Southern Annular Mode (SAM) is also projected to strengthen in austral spring
- There is less consensus among models on projections of frequency change of concurrent (co-occurring) climate driver phases and consecutive ENSO and IOD phases
- Internal variability remains a large source of uncertainty. Multi-model mean results can differ markedly depending on the subset of models used

Supporting Information:

Supporting Information may be found in the online version of this article.

Correspondence to:

C. T. Y. Chung,
christine.chung@bom.gov.au

Citation:

Chung, C. T. Y., Power, S. B., Boschat, G., Gillett, Z. E., & Narsey, S. (2024). Projected changes to characteristics of El Niño-Southern Oscillation, Indian Ocean Dipole, and Southern Annular Mode events in the CMIP6 models. *Earth's Future*, *12*, e2024EF005166. https://doi.org/10.1029/2024EF005166

Received 24 JUL 2024
Accepted 9 OCT 2024
Corrected 3 DEC 2024

This article was corrected on 3 DEC 2024. See the end of the full text for details.

Abstract In this study we analyse projections of future changes to the El Niño Southern Oscillation (ENSO), Indian Ocean Dipole (IOD), and Southern Annular Mode (SAM) using the latest generation of climate models. Multiple future scenarios are considered. We quantify the fraction of models that project future increases or decreases in the frequency and amplitude of ENSO, IOD, and SAM events in the late 21st century. Changes to the frequency of co-occurring and consecutive driver phases are also examined. We find that while there is large inter-model spread, the most common pathways correspond to more frequent ENSO events; weaker, less frequent IOD events; and stronger, but less frequent austral spring SAM events. There is no clear consensus on the change to the frequency of concurrent events, though we find a significant increase in La Niña- and El Niño-only events occurring with neutral IOD and SAM. We also find a significant increase to the frequency of consecutive positive IOD events under a high emissions scenario, but no significant change to the frequency of consecutive ENSO or negative IOD events. In most models, the correlation between drivers, that is, ENSO and IOD, and ENSO and SAM, does not significantly change between the late 20th and late 21st century. These results indicate a high degree of internal variability in the models.

Plain Language Summary Year-to-year climate variability impacts ecosystems and billions of people around the world. Major drivers of this variability in the Southern Hemisphere include the El Niño Southern Oscillation (ENSO), the Indian Ocean Dipole (IOD), and the Southern Annular Mode (SAM). As anthropogenic activities continue to impact the climate, and further change is inevitable, we need to improve understanding of how these climate drivers will change. Here we use the latest generation of climate models to investigate how the strength and frequency of these three climate drivers are projected to change over the remainder of the 21st century. We investigate changes to these drivers individually, as well as changes to the frequency of these drivers occurring simultaneously or consecutively. While there is still a large amount of inter-model spread, the most common model projections are: more frequent ENSO events; weaker and less frequent IOD events; and stronger, but less frequent SAM events. A statistically significant increase in the frequency of consecutive positive IOD events in the high emissions scenario is also found.

1. Introduction

On interannual timescales, the three main modes of variability affecting climate in the tropics and Southern Hemisphere are the El Niño-Southern Oscillation (ENSO) centered in the tropical Pacific, the Indian Ocean Dipole (IOD) in the equatorial Indian Ocean, and the Southern Annular Mode (SAM) in the high southern latitudes (e.g., McPhaden et al., 2020; Saji et al., 1999; Trenberth, 1979 and references within). These modes vacillate between two phases characterized by sea surface temperature anomalies in the Pacific (La Niña and El Niño) and Indian Oceans (positive IOD and negative IOD) or meridional shifts in zonal sea level pressure patterns (positive SAM or negative SAM). These phases strongly influence large-scale temperature and rainfall variability across most of the world (e.g., Cai, Cowan, & Raupach, 2009; Gillett et al., 2023; Hendon et al., 2007; Liguori et al., 2022; Lin & Qian, 2019; R. C. McKay et al., 2023; Risbey et al., 2009; Saji & Yamagata, 2003; Silvestri & Vera, 2003; Yin et al., 2023; Yu et al., 2015).

As the world tracks toward 2– and 3°C of global warming by 2100 relative to preindustrial conditions, and multiple climate tipping points are approached (e.g., D. I. A. McKay et al., 2022 and references within), an increasingly pertinent question is how these modes of variability, and their associated impacts might change. In this study we analyse projections of ENSO, IOD, and SAM from the latest generation of global Coupled General Circulation Models (CGCMs) from the sixth phase of the Coupled Model Intercomparison Project (CMIP6; Eyring et al., 2016). We classify groups of models according to whether they project increases or decreases in climate driver strength and frequency, and identify the most commonly projected changes for each driver. Previous CMIP6-based studies have found a robust projected increase in ENSO-driven SST variability and extreme ENSO events (e.g., Cai et al., 2022) and increases in precipitation variability linked to ENSO in many regions (e.g., Eyring et al., 2021; Power & Delage, 2018). Analysis of large-ensemble models have shown that projected changes to ENSO variability are linked to changes to the tropical Pacific SST gradient (Maher et al., 2023; Rashid, 2022). Projections of IOD change are mixed. An initial study of CMIP5 models found no consensus on IOD change (Hui & Zheng, 2018). However, a closer investigation of CMIP5 and CMIP6 models which were able to simulate distinct moderate and strong positive IOD (pIOD) events showed a projected increase in strong pIOD events, but a weakening in moderate pIOD events (Cai et al., 2021; Wang, Cai, Santoso, et al., 2024). Recently, analysis of long (1000-year) simulations attempted to disentangle the effects of ENSO variability and greenhouse warming on IOD variability, finding a decrease in IOD variability in response to global warming (Kim et al., 2024). Projections of SAM to the end of the 21st century are complicated by whether the strong observed positive trend attributed to greenhouse warming will be offset by ozone recovery, which has the opposing effect (e.g., Zheng, 2023). Previous studies have found a projected poleward shift and strengthening of the Southern Hemispheric westerlies under high emissions scenarios (e.g., Deng et al., 2022).

It is also pertinent to consider projections of concurrent or consecutive occurrences of specific driver phases, and what the impacts of those might be on global and regional climate. Studies so far have indicated that different phases of drivers might respond differently. For example, Geng et al. (2023) found that a subset of CMIP6 models project an increase in consecutive La Niña events by up to 33% under a high emissions scenario. On the other hand, Wang and Cai (2020) found no significant increase in consecutive positive IOD and El Niño co-occurrences.

Our study differs from those listed above in that instead of selecting models that perform well according to a specific metric, we use all available models and all ensemble members for each model. For models with more than one ensemble member, we calculate the ensemble mean so that each model has equal weighting in a multi-model ensemble mean (MMEM). We note that there are advantages and disadvantages to this method. In sampling all models, we weight all models equally regardless of their skill in simulating particular processes. The MMEM may therefore yield different projections to previous studies which only select "highly skilful" models. However the advantage of using all models is that it samples a broader range of possible futures and a more comprehensive estimate of internal variability. We also aim to calculate generalized projections of frequency and amplitude changes for several different climate drivers, so there is no single metric that would apply to ENSO, IOD, and SAM collectively. Additionally, we present here projections of frequency changes of concurrent, and consecutive occurrences of both phases of ENSO and IOD.

2. Data and Methods

In this study, we analyse monthly sea surface temperature (SST) and mean sea level pressure (MSLP) output from 33 CMIP6 models, using all available ensemble members from each model. Output from the last 65 years of Historical, and two Shared Socioeconomic Pathways (SSPs), corresponding to mid-to-high and highest-range emissions future narratives (SSP370 and SSP585; Riahi et al., 2017), are analysed (1950–2014 for Historical, and 2035–2100 for future). The Historical analysis period was started from 1950 to be consistent with previous model evaluation studies (e.g., Chung et al., 2023; Grose et al., 2020). We also utilize output from 200 years of the corresponding pre-industrial control (piC) runs to gauge the statistical significance of forced change. Under the Historical scenario, observed greenhouse gas, ozone, and aerosol forcings are included in the models during the 20th century and early 21st century (Eyring et al., 2016). The SSP370 scenario (which is sometimes referred to as the "Regional Rivalry" scenario) corresponds to a global mean CO_2 concentration of approximately 867 ppm and 4°C of projected warming relative to pre-industrial temperatures by 2100 (Meinshausen et al., 2020). SSP370 also has a distinct high-aerosol emission design which differs from the other SSPs (Shiogama et al., 2023). The SSP585 ("Fossil Fueled Development") scenario corresponds to a global mean CO_2 concentration of

approximately 1,135 ppm and 5°C of projected warming by 2100 (Meinshausen et al., 2020). Meanwhile, the piC runs have greenhouse gases and aerosols fixed at 1850 levels.

ENSO and IOD strength are measured using the Niño 3.4 and Dipole Mode Indices (DMI; Saji et al., 1999) respectively. The Niño 3.4 index is defined as the monthly SST anomalies averaged over the central equatorial Pacific region (5°S–5°N, 170°W–120°W) and the DMI is the difference between SST anomalies averaged over two boxes, one in the western equatorial (50°E−70°E and 10°S–10°N), the other in the south-eastern equatorial (90°E−110°E and 10°S–0°) Indian Ocean. To calculate the SAM index, we use the difference in normalized zonal mean MSLP between 65°S and 40°S (Gong & Wang, 1999; Marshall, 2003). For all indices, anomalies are calculated, and indices are quadratically detrended, relative to the late 21st century (L21C; 2035–2099) and late 20th century (L20C; 1950–2014) respectively.

In this study, we average the indices over December–February (DJF) for Niño3.4, and September–November (SON) for DMI and SAM indices. For Niño3.4 and DMI, DJF, and SON are chosen as these are the seasons when ENSO and IOD events typically peak. SAM varies on sub-seasonal to seasonal timescales but is found to correlate most strongly with ENSO from October to January in observations (Lim et al., 2016). We therefore choose to analyse SAM in SON as this is a season which exhibits strong correlation with ENSO and coincides with the DMI being active. These three drivers have strong impacts on Southern Hemispheric climate in SON (e.g., Chung et al., 2023; Hu et al., 2023).

We here examine the characteristics of ENSO, IOD and SAM separately in the historical and future context, that is, ENSO, IOD, and SAM events are defined to occur when their indices exceed 0.75 standard deviation (SD) in their respective time periods and not just relative to SD in the Historical period. It is important to note here that if the future variability of a driver changes, then SD(L21C) will differ from SD(L20C). For example, if SD(L21C) were to increase relative to SD(L20C), a year which counted as an event in L20C might not be counted in L21C. Conversely if the SD(L21C) were to decrease relative to SD(L20C), then an event counted in L21C might not be counted as an event in L20C. We note that this differs from some previous studies which characterize changes based on a historical baseline (e.g., Cai et al., 2022; Kim et al., 2024). We adopt this alternative approach to show how ENSO, IOD, and SAM events are projected to change, based on events as they might be defined in the future. In this study we also examine how projected changes to the strength of events is related to the change in SD.

There is an assumption here that using 0.75SD is an equally valid event threshold in both periods. For consistency, the same subset of models and ensemble members are used for Historical, SSP370 and SSP585 comparisons (listed in Table S1 in Supporting Information S1). Due to data availability, a total of 185 runs from 33 models are used for ENSO and IOD analysis as both indices are derived from SSTs. For SAM analysis, 205 runs from 31 models, since there are fewer available models with MSLP output from all three scenarios to derive the SAM index.

To determine whether future changes are statistically significant, we compare the forced change (L21C-L20C) to the "unforced" change which we estimate in two separate and detrended 65-year piC periods using the last 200 years available from each piC run. Assuming that any change in frequency or amplitude from the piC runs is purely due to the models' internal variability, comparing two periods from the piC provides an estimate of this. Differences outside the 95% confidence interval calculated from this range are then assumed to be very likely due to the increase in external forcing. For the piC, the first available runs from 54 models are used for ENSO, IOD, and SAM.

3. Results

3.1. Projected Changes to Frequency and Strength of ENSO, IOD, and SAM

We quantify the projected changes to the drivers in two ways: (a) significant change in frequency (ΔFrequency), and (b) significant change in amplitude (ΔAmplitude). To calculate changes in the frequency of each driver, the sum of events over the L21C and the L20C periods are compared. For changes in strength, we compare the amplitudes of L21C and L20C driver indices. We discuss changes to separate (i.e., positive and negative) phases of each driver, noting again that only events with indices exceeding 0.75SD are chosen, and the SD is calculated separately for L20C and L21C.

10.1029/2024EF005166

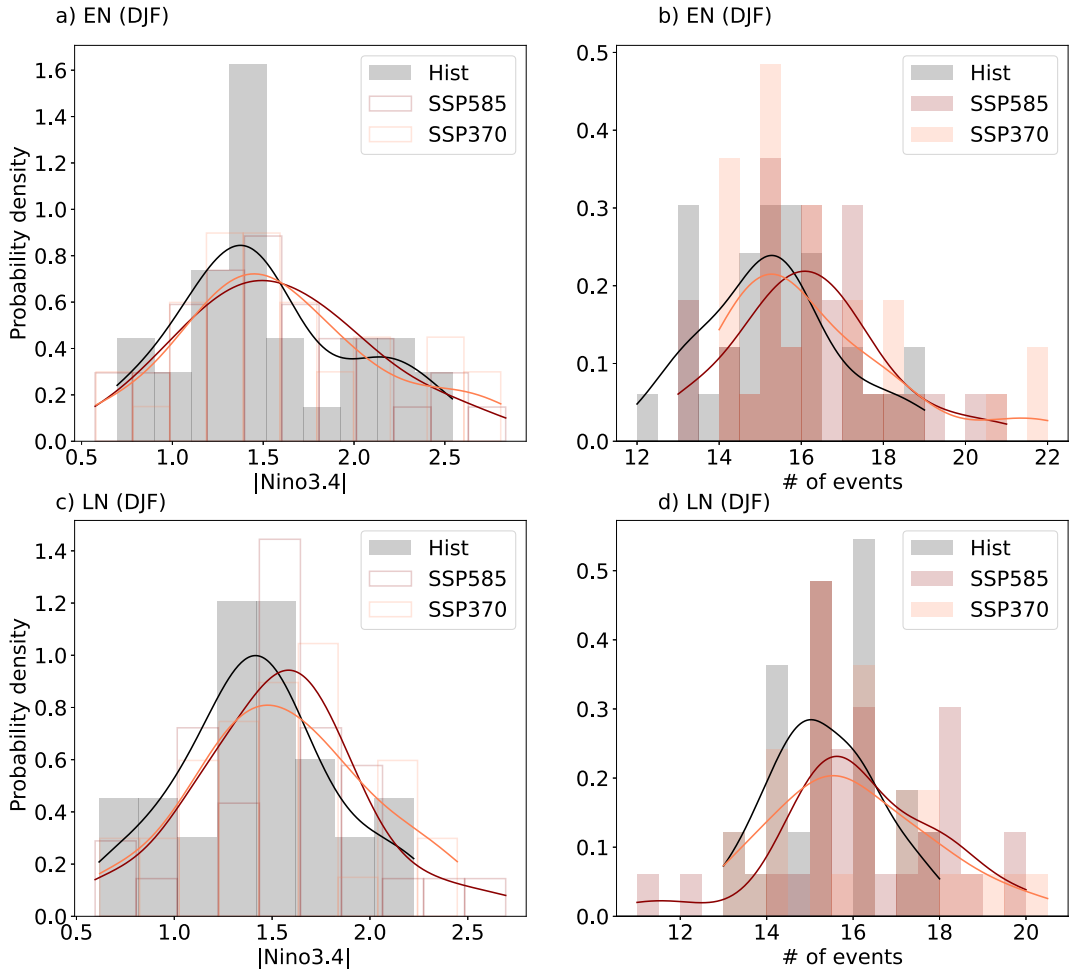

Figure 1. Distributions of strength and frequency of EN and LN events for Historical, SSP585 and SSP370 scenarios. (a) Normalized histogram of absolute value of DJF Niño3.4 for EN events, averaged over L20C for Historical (black), and L21C for SSP370 (orange) and SSP585 (red) scenarios. (b) Normalized histogram of number of EN events for averaged over L20C for Historical, and L21C for SSP370 and SSP585 scenarios. In (a) and (b), filled orange and red bars indicate that the mean difference (L21C—L20C) is significant at the 90% level according to a *t*-test, hollow bars indicate that the difference is not significant. Smooth curves show the kernel density estimate (continuous probability density curve) of best fit for each of the distributions. (c andd) The same as in (a and b), but for LN events. Future scenarios correspond to L21C and Historical corresponds to L20C (see text for included years). For models with multiple ensemble members, the MEM is used.

3.1.1. ENSO

In the following analysis we consider two main properties: the shift in the mean distribution of ΔAmplitude or ΔFrequency change, and the fraction of models which project changes that may be larger than expected from internal variability. To address the first property, distributions of L20C and L21C amplitude and frequency are shown for El Niño (EN) events (Figures 1a and 1b) and La Niña (LN) events (Figures 1c and 1d). For each model with multiple ensemble members, the ensemble mean is used, ensuring that each model is equally weighted in the comparison.

We first discuss mean shifts in the distribution of the amplitude. For EN events, Figure 1a shows a normalized histogram of the absolute value of the DJF Niño3.4 index averaged over L20C for Historical (black), and L21C for SSP370 (orange) and SSP585 (red) scenarios, with similar results shown for LN events in Figure 1c. It is also important to note that approximately 66% of models show an increase in Niño3.4 SD (ΔSD) in the future (Figure S1a in Supporting Information S1), which indicates an overall increase in ENSO variability (consistent with previous results of Cai et al., 2022). This means that the events selected as EN/LN events in L21C would generally have a slightly larger amplitude, using our >0.75 SD threshold. While the SSP370 and SSP585 distributions show

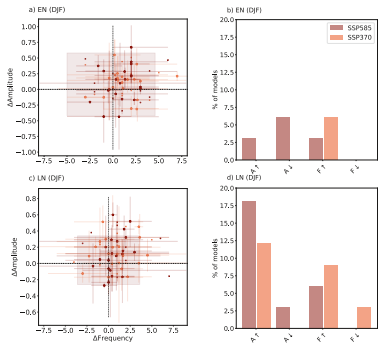

Figure 2. Projected changes to the strength and frequency of EN and LN events for SSP585 and SSP370. (a) ΔAmplitude versus ΔFrequency for SSP370 (orange) and SSP585 (red) scenarios for EN events. For models with multiple ensemble members, the multi-ensemble means are denoted as stars, with the spread from individual ensemble members shown as whiskers around the stars. Models with only one 1 ensemble member are denoted by squares. The tan box shows the 95% confidence interval of ΔAmplitude and ΔFrequency from the piControl runs indicating internal variability. (b) The fraction of models which lie outside the tan box, showing changes that are increasing (↑) or decreasing (↓). (c and d) The same as in (a and b), but for LN events. Future scenarios correspond to L21C and Historical corresponds to L20C (see text for included years).

a slight shift toward larger amplitudes of Niño 3.4, a *t*-test indicates that the change in means of both future and historical distributions are not statistically significant at the 90% level. A regression map of ΔAmplitude against SST ΔSD at every grid point across models suggests that models with greater SST variability increase (larger ΔSD) across the equatorial Pacific and North Tropical Atlantic oceans display larger ΔAmplitude in ENSO events (Figures S1b and S1c in Supporting Information S1).

Secondly, we examine mean shifts in the normalized hisograms of the number of EN events (Figure 1b) and LN events (Figure 1d) averaged over L20C and L21C periods. Both EN and LN events show a moderate increase in the frequency of future events, with the mean increase in EN frequency being statistically significant for both SSP370 and SSP585, and the mean increase in LN frequency being only significant for SSP585.

Having identified the mean shift in amplitude and frequency distributions, we now examine the consensus amongst models on the sign and strength of change and also estimate how much of these changes might be expected from internal, or unforced, variability. Figures 2a and 2c show a scatter plot of ΔAmplitude versus ΔFrequency for EN and LN events, respectively. Each multi-ensemble mean is marked by a star, with whiskers denoting the spread of individual ensemble members and squares indicating single-ensemble models. To estimate the spread of change expected from internal variability, we also calculate ΔAmplitude and ΔFrequency for two independent 65-year periods in the piC simulations. The tan boxes in Figures 2a and 2c highlight the 95% confidence interval estimated from the piC runs. Interestingly, the range of this internal variability is approximately 50% larger for EN years compared to LN years, in both amplitude and frequency. Both are also skewed toward positive ΔAmplitude.

Using this criteria for internal variability, we then calculate the fraction of models which project ΔAmplitude or ΔFrequency that lie outside the tan box. For EN years (Figure 2b), very few models lie outside the box, with only two models in SSP370 (6% of all models) and one model in SSP585 (3%) showing a frequency increase outside the piC box. Two SSP585 models lie just below the bottom edge of the piC box indicating an amplitude decrease, and one lies above indicating amplitude increase. For LN years (Figure 2d) these numbers are generally larger due to the combination of reduced internal variability compared to EN years, and a larger increase in amplitude projected in some models. Approximately 18% of SSP585 models and 12% of SSP370 models show an increase in LN amplitude. 10% of SSP370 models and 6% of SSP585 show an increase in frequency. Note that these fractions are calculated using the MEMs; if we were to consider individual runs instead, the fraction of runs lying outside the piC box would be considerably higher (assuming each run to be weighted equally).

Overall, these results indicate that while a mean shift in the EN and LN mean frequency distributions may be statistically significant, the majority of models project ΔFrequency to lie within the bounds of the piC simulations that is, changes expected from internal variability. Conversely, while 12%–18% of models project a percentage of ΔAmplitude larger than internal variability for LN events, the shift in the mean amplitude distribution is not statistically significant.

3.1.2. IOD

For the IOD, there is less consensus amongst models on the change in variability, with approximately half the models indicating an increase in SD, and half indicating a decrease (Figure S2a in Supporting Information S1). Figures 3a and 3c show the normalized histograms of absolute values of SON DMI for positive (pIOD) and negative IOD (nIOD) events respectively, averaged over the L20C and L21C periods. Unlike for ENSO, we find that there is a statistically significant decrease in the mean of the amplitude distributions of both pIOD and nIOD in SSP585. SSP370 however shows a significant decrease for nIOD events only.

In terms of frequency changes, Figures 3b and 3d depict no significant changes in the means of these histograms of number of events averaged over L20C and L21C for either pIOD or nIOD. The nIOD frequency distributions

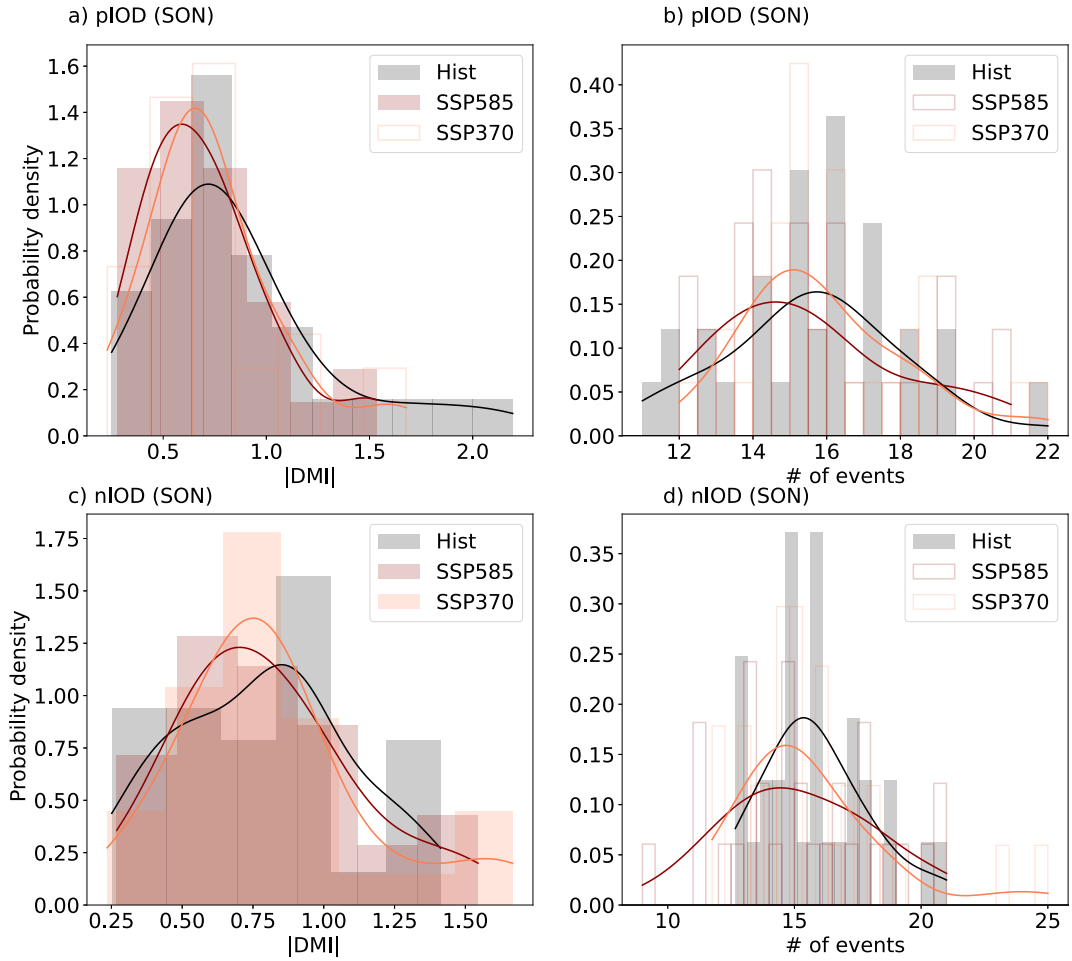

Figure 3. Distributions of strength and frequency of pIOD and nIOD events for Historical, SSP585 and SSP370 scenarios. (a) Normalized histogram of absolute value of SON DMI for pIOD events, averaged over L20C for Historical (black), and over L21C for SSP370 (orange) and SSP585 (red) scenarios. (b) Normalized histogram of number of pIOD events averaged over L20C for Historical, and L21C for SSP370 and SSP585 scenarios. In (a) and (b), filled orange and red bars indicate that the mean difference (L21C—L20C) is significant at the 90% level according to a *t*-test, hollow bars indicate that the difference is not significant. Smooth curves show the kernel density estimate (continuous probability density curve) of best fit for each of the distributions. (c and d) The same as in (a and b), but for nIOD events. Future scenarios correspond to L21C and Historical corresponds to L20C (see text for included years). For models with multiple ensemble members, the MEM is used.

for SSP370 and SSP585 exhibit a higher number of outliers compared to the Historical distribution. Specifically, the tail of the SSP370 distribution extends 25% higher than Historical, while the tail of the SSP585 distribution extends 25% lower.

We now consider the scatter plots of ΔAmplitude and ΔFrequency for pIOD and nIOD (Figures 4a and 4c), comparing the SSP370 and SSP585 changes to those estimated in the piC runs. Unlike for ENSO, the extent of the piC box for IOD is relatively similar for pIOD and nIOD years, with a small skewness toward decreasing amplitude. The range of the piC box is also smaller than for ENSO, indicating less internal variability associated with IOD changes in the models.

Again, using this criteria, we calculate the fraction of models showing ΔAmplitude and ΔFrequency which lie outside the box. The fraction of models in each category is markedly different for pIOD and nIOD events.

For pIOD, approximately 35%–40% of models in both scenarios show an amplitude decrease larger than can be expected from internal variability (Figure 4b). Meanwhile, 25% of models in both scenarios show frequency increases. Less than 10% of models in both scenarios fall into the other pathways (amplitude increase or frequency decrease). Contributing to these amplitude decrease/frequency increase fractions are a cluster of models (CAS-

10.1029/2024EF005166

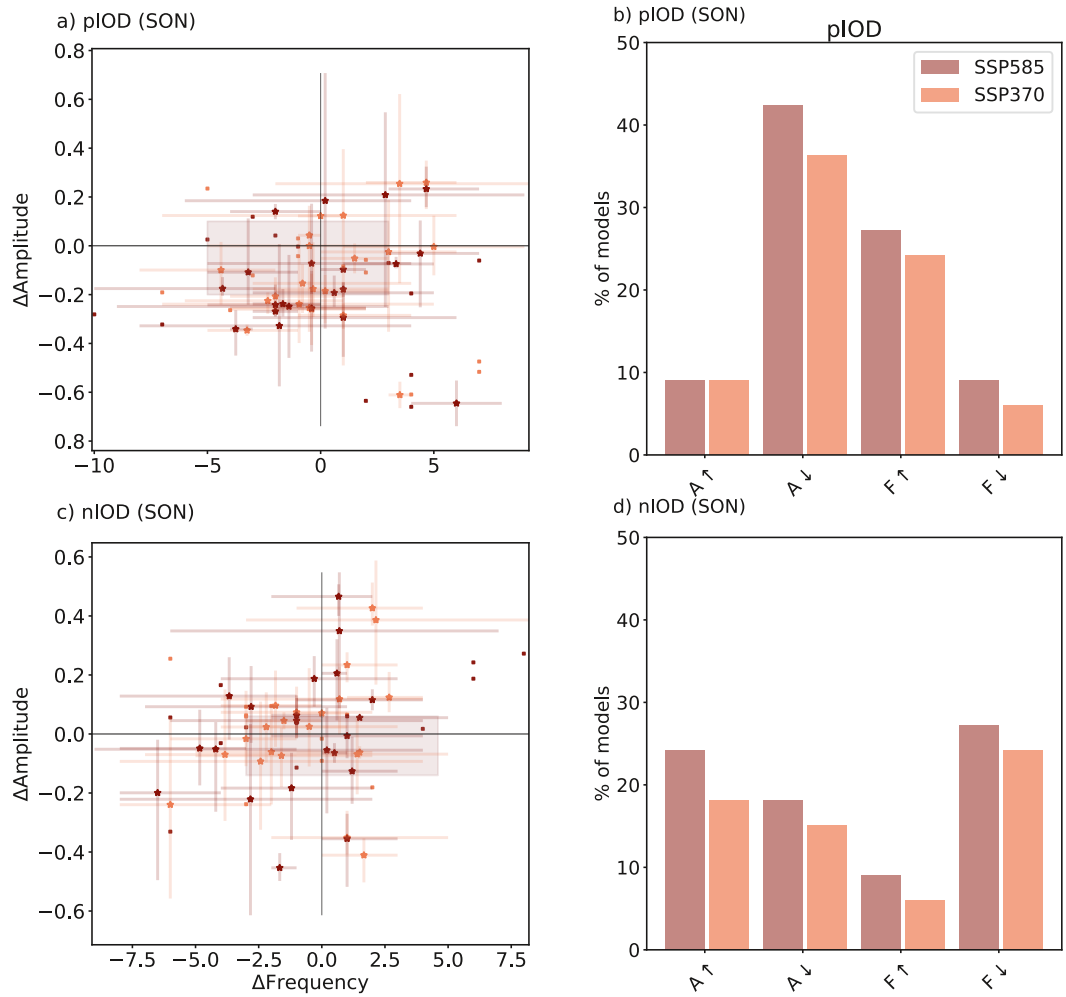

Figure 4. Projected changes to the strength and frequency of pIOD and nIOD events for SSP585 and SSP370. (a) ΔAmplitude versus ΔFrequency for SSP370 (orange) and SSP585 (red) scenarios for pIOD events. For models with multiple ensemble members, the multi-ensemble means are denoted as stars, with the spread from individual ensemble members shown as whiskers around the stars. Models with only one 1 ensemble member are denoted by squares. The tan box shows the 95% confidence interval of ΔAmplitude and ΔFrequency from the piControl runs indicating internal variability. (b) The fraction of models which lie outside the tan box, showing changes that are increasing (↑) or decreasing (↓). (c and d) The same as in (a and b), but for nIOD events. Future scenarios correspond to L21C and Historical corresponds to L20C (see text for included years).

ESM2-0, CMCC-ESM2, FGOALS-f3-L for both scenarios, and ACCESS-ESM1.5 for SSP585 only), with a noticeably large amplitude decrease in the bottom right quadrant of the scatter plot (Figure 4a).

The model consensus is different for nIOD events, with more of a mixed response in ΔAmplitude (Figure 4d). 18%–25% of models in both scenarios show an amplitude increase, and 15%–18% show an amplitude decrease. Over 25% of models in both scenarios show a frequency decrease, while 7%–10% show an increase. Therefore, the "most common" future projection for pIOD events involves weaker but more frequent events. For nIOD events, there is less consensus on the amplitude change, but more models indicate stronger, less frequent events.

Investigating this asymmetry between pIOD and nIOD changes, there is a difference between projected DMI changes which depends on the strength of the DMI averaged over the historical period (Figures S2d and S2e in Supporting Information S1). For pIOD events, there is a strong tendency for runs which have a weaker historical DMI to strengthen, and runs which have a stronger historical DMI to weaken. For nIOD events, there is only a tendency for runs which start off weak to strengthen, with more of a mixed signal for runs which start off strong.

Though further work is required to understand the mechanisms behind this, it explains, in part, more models projecting a weakening of pIOD events than nIOD events.

There is also an interesting cross-model relationship between ΔAmplitude and SST ΔSD at every grid point (Figures S2b and S2c in Supporting Information S1). For pIOD, ΔAmplitude is significantly correlated to SST ΔSD in the eastern equatorial Indian Ocean and western equatorial Pacific, suggesting that models simulating a strong increase in SST variability in these regions (and not necessarily in the western Indian Ocean), would also tend to project an increase in pIOD amplitude. For nIOD, ΔAmplitude is correlated with SST ΔSD in the eastern equatorial Indian Ocean but also across large areas of the North Pacific and North Atlantic sectors. While fully understanding the reason behind this large difference in phases requires further work, we also test whether this behavior is linked to the models' overall warming trend, see discussion in Section 4.1.

3.1.3. SAM

The different phases of SAM capture the strength and position of the mid-latitude westerly winds in the Southern Hemisphere, with positive phases (pSAM) promoting a poleward shift and intensification of the circumpolar westerly belt and associated storm tracks, and opposite tendencies for negative SAM (nSAM). Previous studies have shown that CMIP6 models project the westerly winds to strengthen and move southward in all seasons by the end of the L21C under high emission scenarios, with the largest of these positive SAM-like trends expected under SSP585 (Deng et al., 2022; Goyal et al., 2021). However, our analysis focuses on change in the amplitude and frequency of events, which is why we have detrended the SAM indices and identified events according to L20C and L21C SDs separately, allowing us to compare the characteristics of SAM events during the historical period to a future climate.

We find that the projected changes in amplitude and frequency distributions of SON SAM display the most robust changes of the three drivers considered here. In particular, there is a significant shift toward stronger SAM events for both SSP370 and SSP585 scenarios. The means of the normalized histograms of SAM index amplitude, averaged over L20C and L21C, increase by approximately 30% (Figures 5a and 5c). There is also a statistically significant shift toward fewer SAM events by L21C (Figures 5b and 5d). These results would therefore suggest fewer (positive and negative) SAM events but of larger excursions in the future. Note that as we are defining the SAM index to be the difference between the zonal mean MSLP between 60°S and 45°S, a larger amplitude means a stronger pressure gradient between these two latitudes.

A large fraction of these changes also lie outside the range of internal variability, with 15%–20% of models located in the top left quadrant of Figures 6a and 6c, indicating stronger but fewer events in the future. Approximately 37%–55% of models project stronger pSAM and nSAM amplitudes, while 15%–20% project less frequent events (Figures 6b and 6d).

In terms of overall variability, most models project an increase in the SON SAM index variability (Figure S3a in Supporting Information S1). Not surprisingly however, unlike ENSO or IOD, the change in SAM strength is not significantly correlated with a change in SST variability (ΔSD) in any region in the tropics or extratropics (Figures S3b and S3c in Supporting Information S1). In Section 4 we show how it is instead related more closely to the mean state change in the SSTs.

To summarize the projected changes to drivers, our results show that there is a mean increase in ENSO frequency and no significant change in mean ENSO strength. However, very few models exhibit a frequency change which exceeds the range of internal variability. 15% of models indicate a degree of LN amplitude increase outside the range of internal variability, whereas only one model does so for EN. Projections for the IOD indicate an overall decrease in strength, but no significant change in overall frequency. In terms of changes exceeding internal variability, pIOD and nIOD phases show differing projections. For pIOD, 35% of models exhibit a weakening of pIOD, and 25% of models exhibit a frequency decrease. For nIOD, a similar fraction of models (15%–25%) show strengthening and weakening, while 30% of models show a decrease in events. Only SAM shows a relatively robust change in terms of model agreement, with approximately 50% of models indicating an increase in amplitude and 20% of models indicating a decrease in events for both pSAM and nSAM phases.

Projections from SSP370 and SSP585 are very similar in terms of the spread of ensemble members and overall distributions of amplitude and frequency change.

10.1029/2024EF005166

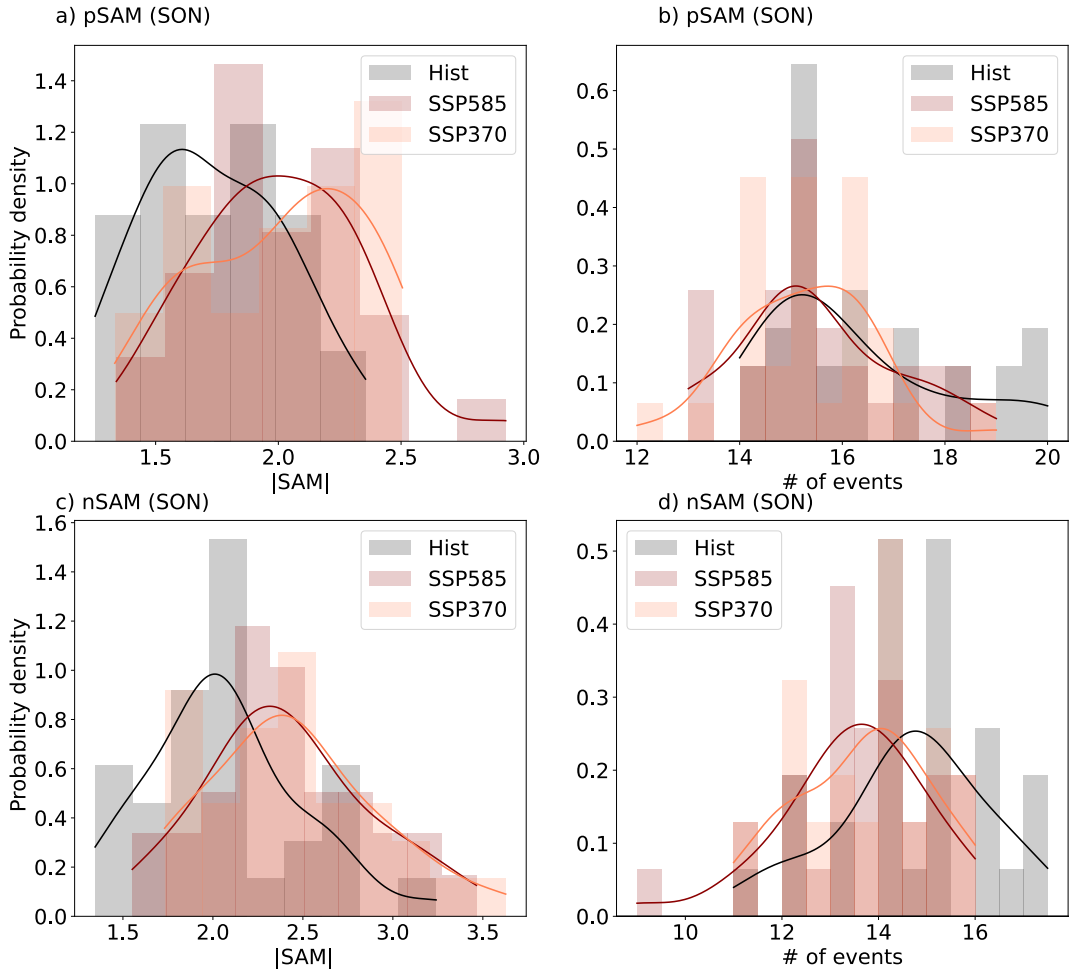

Figure 5. Distributions of strength and frequency of pSAM and nSAM events for Historical, SSP585 and SSP370 scenarios. (a) Normalized histogram of absolute value of the SON SAM index for pSAM events, averaged over L20C for Historical (black), and L21C for SSP370 (orange) and SSP585 (red) scenarios. (b) Normalized histogram of number of pSAM events averaged over L20C for Historical, and L21C for SSP370 and SSP585 scenarios. In (a) and (b), filled orange and red bars indicate that the mean difference (L21C—L20C) is significant at the 90% level according to a *t*-test, hollow bars indicate that the difference is not significant. Smooth curves show the kernel density estimate (continuous probability density curve) of best fit for each of the distributions. (c and d) The same as in (a-b), but for nSAM events. Future scenarios correspond to L21C and Historical corresponds to L20C (see text for included years). For models with multiple ensemble members, the MEM is used.

3.2. Projected Changes to Frequency of Concurrent Drivers

We next look at the projected changes to the frequency of occurrences of concurrent phases of drivers. Since 1950, there have been multiple observed co-occurrences of La Niña (LN), negative IOD, and positive or negative SAM (pSAM/nSAM), as well as El Niño (EN), positive IOD, and pSAM or nSAM. The compounding influence of these phases, such as in 2019, 2021, and 2022, have likely contributed to the severity of drought or floods such as those which occurred over Australia (e.g., Huang et al., 2024; Reddy et al., 2022; Wang & Cai, 2020). Note that ENSO and the IOD are strongly correlated, and no occurrences of EN and negative IOD have been observed over this time period. LN and positive IOD events are extremely rare (e.g., Behera et al., 2008; Cai, Cowan, & Raupach, 2009; Cai, Pan, et al., 2022).

Consistent with the mixed results in projected frequency changes, particularly for IOD, there is no obvious trend for changes to the frequency of concurrent ENSO, IOD, and SAM phases. Figure 7 shows normalized histograms of the number of LN events occurring concurrently with both negative or neutral IOD and pSAM, nSAM or neutral SAM. Figure 8 shows the same for EN events occurring concurrently with both positive or neutral IOD

10.1029/2024EF005166

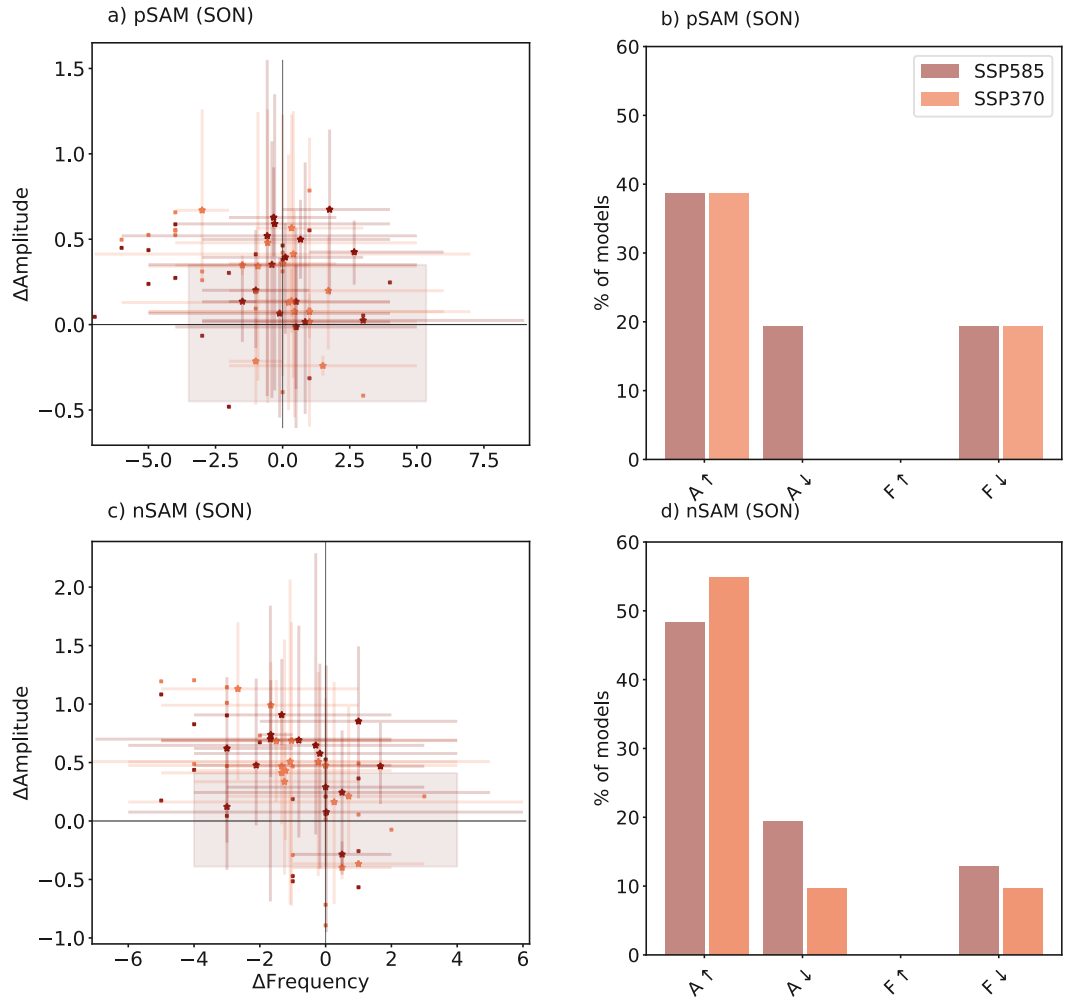

Figure 6. Projected changes to the strength and frequency of pSAM and nSAM events for SSP585 and SSP370. (a) ΔAmplitude versus ΔFrequency for SSP370 (orange) and SSP585 (red) scenarios for pSAM events. For models with multiple ensemble members, the multi-ensemble means are denoted as stars, with the spread from individual ensemble members shown as whiskers around the stars. Models with only one 1 ensemble member are denoted by squares. The tan box shows the 95% confidence interval of ΔAmplitude and ΔFrequency from the piControl runs indicating internal variability. (b) The fraction of models which lie outside the tan box, showing changes that are increasing (↑) or decreasing (↓). (c and d) The same as in (a and b), but for nSAM events. Future scenarios correspond to L21C and Historical corresponds to L20C (see text for included years).

and pSAM, nSAM, or neutral SAM. Solid bars indicate that the normalized histograms for SSP370 or SSP585 have a significantly different mean from Historical at the 90% level according to a *t*-test.

We discuss here only the statistically significant mean changes. For La Niña and nIOD combinations, the only significant change is in the frequency of LN/nIOD/nSAM events under SSP370, with a mean increase of 52% compared to the Historical period (Figure 7b). The number of concurrent LN/neutral IOD/pSAM events decreases on average by 35% under SSP585 respectively (Figure 7b), while the number of LN-only (with neutral IOD/neutral SAM) events, increases on average by 13% under SSP370 (Figure 7b).

For concurrent events involving El Niño, the projected changes are less significant (Figure 8). The only significant change is a mean 17%–18% increase in EN-only (neutral IOD/neutral SAM) events (Figure 8f).

Reflecting the uncertainty in frequency change in most drivers seen in Figures 1–6, the spread of the distributions in Figures 7 and 8 imply that there is also a large degree of uncertainty in projected changes in the frequency of concurrent driver events. In some cases, the degree of consistency among models in projections also differs by

10.1029/2024EF005166

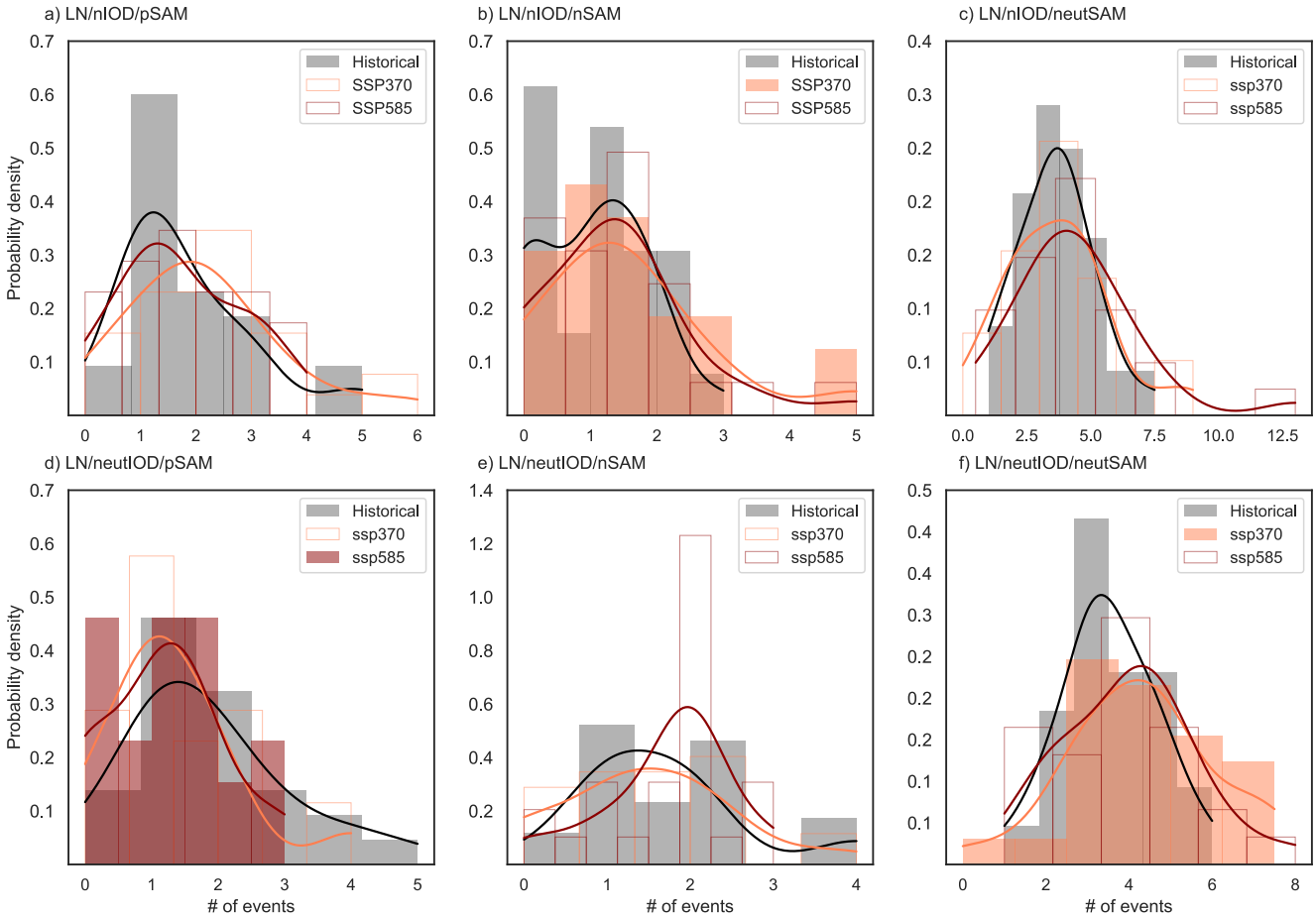

Figure 7. Changes in frequency of the concurrent events involving La Niña, nIOD and neutral IOD phases, and distinct phases of SAM. (a) Bars show normalized histograms of the number of events of concurrent La Niña/negative IOD/positive SAM events for L21C under SSP585 (red) and SSP370 (orange) relative to Historical (L20C). Smooth curves show the kernel density estimate (continuous probability density curve) of best fit for each of the distributions. The following panels show the same, but for (b) La Niña/negative IOD/negative SAM events, (c) La Niña/negative IOD/neutral SAM events, (d) La Niña/neutral IOD/positive SAM events, (e) La Niña/neutral IOD/negative SAM events, and (f) La Niña/neutral IOD/neutral SAM events Solid bars indicate where the means of the distributions are statistically significant at 90% according to a *t*-test.

scenario. Nevertheless, there are several combinations which yield significantly different distribution means. Under SSP370, models project significant increases in the number of LN/nIOD/nSAM events, LN-only and EN-only events. Under SSP585, models project significant increases to the number of LN/neutral IOD/pSAM, and EN-only events.

3.3. Projected Changes to Consecutive Phases of ENSO and IOD

We now extend the analysis to examine projections of consecutive occurrences of the same driver phases, that is, two or more EN, LN, pIOD or nIOD. As demonstrated by the recent triple (back-to-back-to-back) La Niñas of 2020–22 and consecutive negative IOD event of 2020–21, the recurrence of anomalously wet conditions in Australia can impact soil saturation and water catchment levels, exacerbating the extent of floods (e.g., Huang et al., 2024; Jeong et al., 2023). On the other hand, events such as the consecutive El Niño/pIODs of 2018–2019 can exacerbate extreme hot and dry conditions in Australia, leading to drought (Okumura et al., 2017; Wang & Cai, 2020; Yin et al., 2022).

Figure 9 shows the multi-model mean of the number of consecutive EN, LN, pIOD, and nIOD events, for Historical, SSP370 and SP585 scenarios. Again, for models with more than one ensemble member, we have used the multi-ensemble mean. To test statistical significance in the change in number of events, we show the standard deviation of 9999 bootstrapped samples of the consecutive event count per model in each scenario. In doing so,

10.1029/2024EF005166

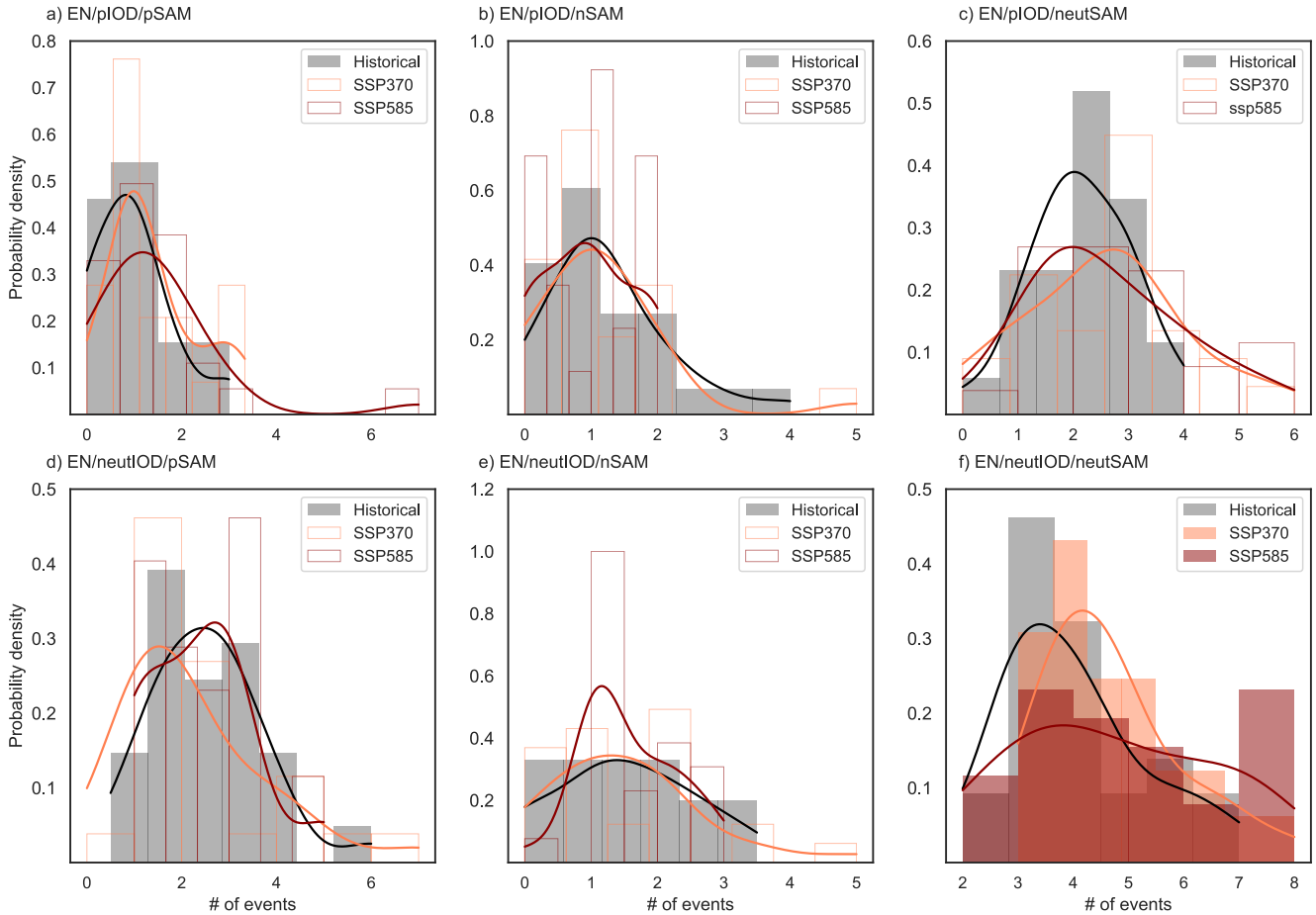

Figure 8. Changes in frequency of concurrent events involving El Niño, positive and neutral IOD, pSAM and nSAM. (a) Bars show the normalized histograms of the number of events of concurrent El Niño/positive IOD/positive SAM events for L21C under SSP585 (red) and SSP370 (orange) relative to Historical (L20C). Smooth curves show the kernel density estimate (continuous probability density curve) of best fit for each of the distributions. The following panels show the same, but for (b) El Niño/positive IOD/negative SAM events, (c) El Niño/positive IOD/neutral SAM events, (d) El Niño/neutral IOD/positive SAM events, (e) El Niño/neutral IOD/negative SAM events, and (f) El Niño/neutral IOD/neutral SAM events. Solid bars indicate where the means of the distributions are statistically significant at 90% according to a *t*-test.

the only statistically significant change seen is a 23% increase in consecutive pIOD events under SSP585 (Figure 9c). While Figure 9b shows a small increase in consecutive LN and Figure 9d shows a decrease in consecutive nIOD events, these are not statistically significant.

A recent study selected a subset of models which performed best in simulating tropical Pacific SST skewness and found that these models exhibit a significant increase in the frequency of consecutive La Niñas (comparing 2000–2099 and 1900–1999), while other models did not necessarily do so (Geng et al., 2023). We also note again that our future events are selected according to an L21C baseline. This highlights how the model selection method, as well as baseline selection, in evaluating any particular metric can significantly impact the conclusions drawn from any projection analysis.

4. Avenues for Further Research

In Section 3, and Figures S1–S3 in Supporting Information S1, we showed that models with larger variability change in the tropical Pacific tended to show a larger increase in EN/LN amplitude. Models with larger variability change in the northern hemisphere SSTs tended to show larger increase in nIOD amplitude, whereas the change in pSAM/nSAM amplitude did not correlate with variability change. To fully understand the reasons behind these projected changes, a more thorough investigation into the individual model's behavior is required. Although this is outside the scope of this study, in this section we explore a few metrics which may inform future work. We briefly

10.1029/2024EF005166

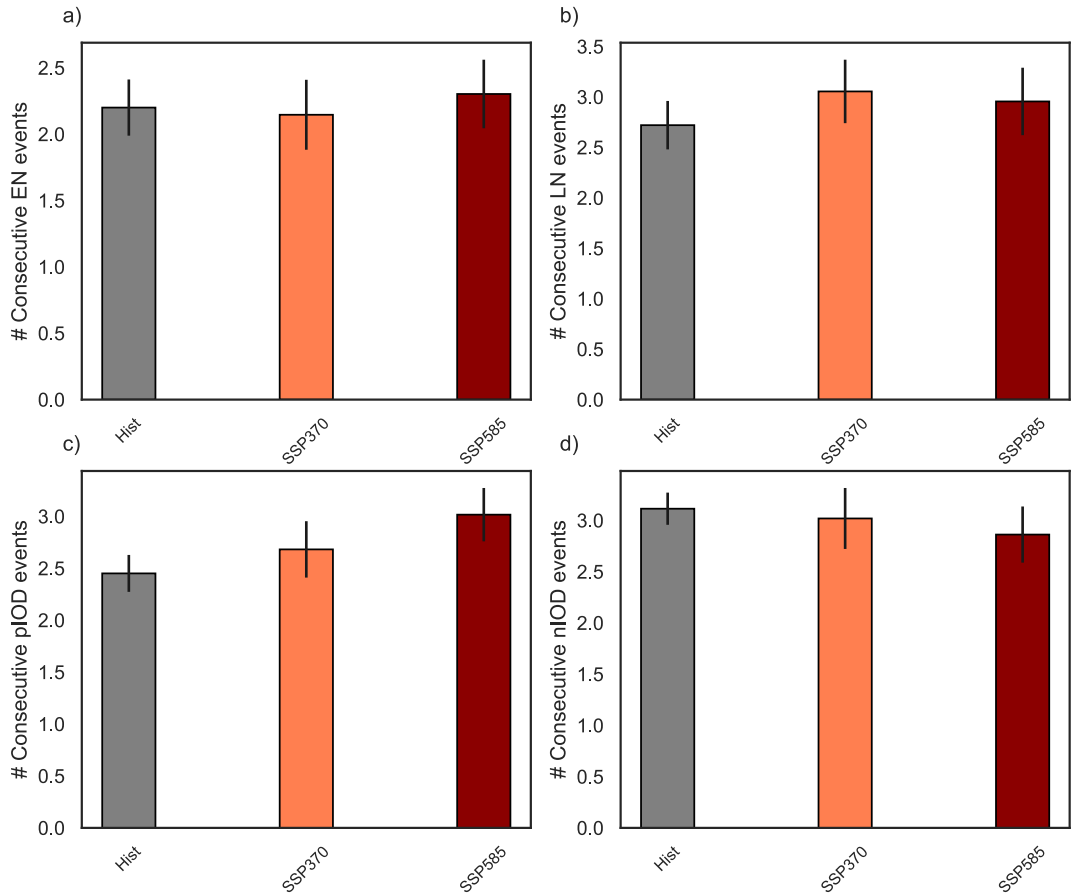

Figure 9. Frequency of co-occurrences (average number of events per model run) of two or more consecutive (a) El Niño, (b) La Niña, (c) positive IOD, and (d) negative IOD events for Historical (L20C), SSP370, and SSP585 (L21C) scenarios. Error bars indicate 1 standard deviation of 9999 bootstrapped samples.

look at whether there is a relationship between the projected changes to the drivers and the models' warming trend. We also show how the relationship between drivers is projected to change.

4.1. Driver Changes and SST Trend

As noted in Section 3, in some models there is a difference in the projected ΔAmplitude and ΔFrequency for separate driver phases, for example, the varying responses in pIOD and nIOD amplitude change. To better understand this, we regress across models ΔAmplitude and ΔFrequency against their associated SST change at each grid point. The SST (warming) pattern is calculated as the difference in mean L21C and L20C SSTs. As this analysis is just exploratory, we focus only on SSP585.

Figure 10 shows the model-to-model relationship between ΔAmplitude and the degree of SST change and highlights some interesting differences in the response of positive and negative driver phases. Stippling in the maps indicates that models exhibit a statistically significant relationship between the degree of driver amplitude change they simulate and the degree of SST warming they project. For example, the projected change to EN amplitude is negatively correlated (or inversely related) to the SST change simulated over much of the Southern Ocean as well as the eastern equatorial Pacific (Figure 10a), while the changes to LN amplitude (Figure 10d) are positively correlated with northern tropical Atlantic SST warming. This implies that models with a larger degree of warming in the Southern Ocean tend to project a decrease in EN amplitude, while models with a larger degree of warming in the northern tropical Atlantic tend to project an increase in LN amplitude. It also suggests that models with a stronger warming in the equatorial eastern Pacific (i.e., a more "El Nino-like" warming pattern) project a decrease in EN amplitude, implying that some of the mean-state and interannual variability changes are anticorrelated in models.

10.1029/2024EF005166

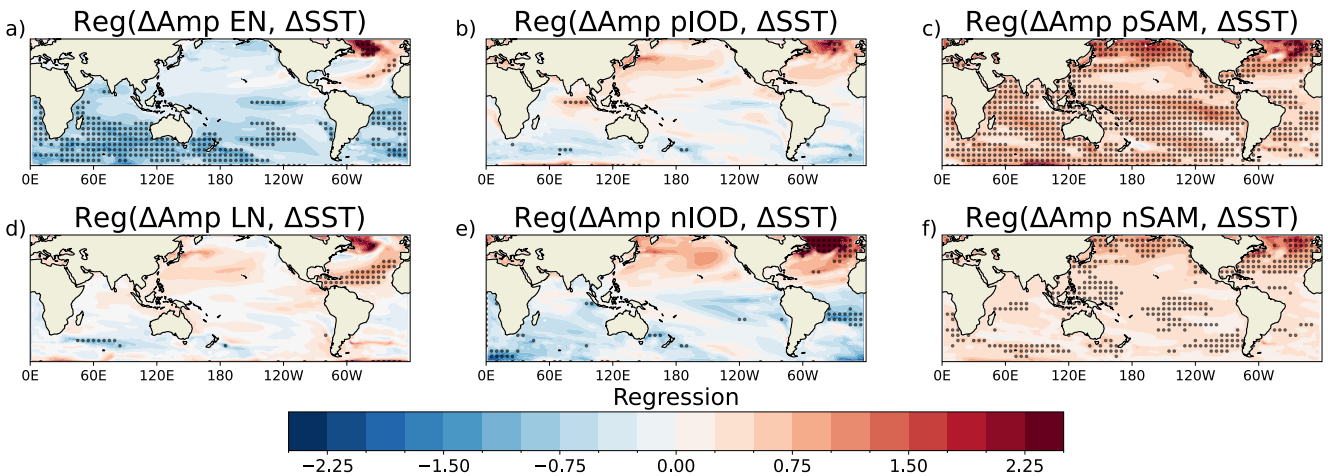

Figure 10. Regression coefficients of ΔAmplitude against the SST warming pattern for (a) EN, (b) pIOD, (c) pSAM, (d) LN, (e) nIOD, (f) nSAM phases under SSP585. Stippling shows where regression is significant at the 90% level.

For the IOD, the changes in the SST in the eastern pole are more linked to IOD amplitude than the western pole. pIOD amplitude change is only significantly correlated with a small region of eastern Indian Ocean warming, whereas nIOD amplitude change is correlated positively with warming in the north Atlantic and negatively with warming in the south Atlantic (Figures 10b and 10e). Meanwhile, Figure 10c implies that pSAM amplitude change is larger in models with larger warming across the tropics. For nSAM, the relationship is similar but less robust (Figure 10f).

While these results, and those from Figures S1–S3 in Supporting Information S1. Require further work to fully understand, they imply the change in ENSO and IOD event amplitudes are more correlated with the change in local SST variability, rather than mean state change, in the models. Meanwhile, change in SAM event amplitudes are more correlated with the global mean state change in SST, rather than localized variability. Some interesting questions are also raised as to why EN event amplitude is negatively correlated with ΔSST in the Southern Ocean, or why nIOD event amplitude is positively correlated with SST variability change in the North Pacific and North Atlantic. While the details of these are outside the scope of the current study, these figures highlight some key areas to explore as they relate the model mean state SST changes to the changes they project in the characteristics of specific driver phases.

4.2. Changes to Driver Interactions

The results in Section 3 show that while the change in ENSO amplitude is still largely within the range of internal variability, some models show a significant increase in LN amplitude. However, a fraction of models also project a weakening of pIOD and nIOD events. This is somewhat surprising as ENSO and the IOD are typically highly correlated. We therefore show here how the correlation between Niño3.4 and DMI, and Niño3.4 and SAM is projected to change between L20C and L21C.

In Figures 11a and 11b, the correlation between drivers is indicated by crosses, sorted from lowest to highest Historical values. This can be compared to the changes to driver correlations for the piControl models in Figure S4 in Supporting Information S1. For the ENSO-IOD correlation, approximately 66% of models project a strengthening of their Historical correlation (regardless of sign) across both future scenarios. In the piControl runs, 55% of models project an increase. The degree of change in the correlation coefficients however, lie within the range of internal variability for all but three models.

Approximately 65% of models show a decrease in the ENSO-SAM correlation across both future scenarios (compared to 46% for piControl). In this case, none of the models display a degree of change that lie outside the range of internal variability. However, in general, models poorly capture the observed SAM-ENSO relationship and its seasonal variation (Lim et al., 2016).

10.1029/2024EF005166

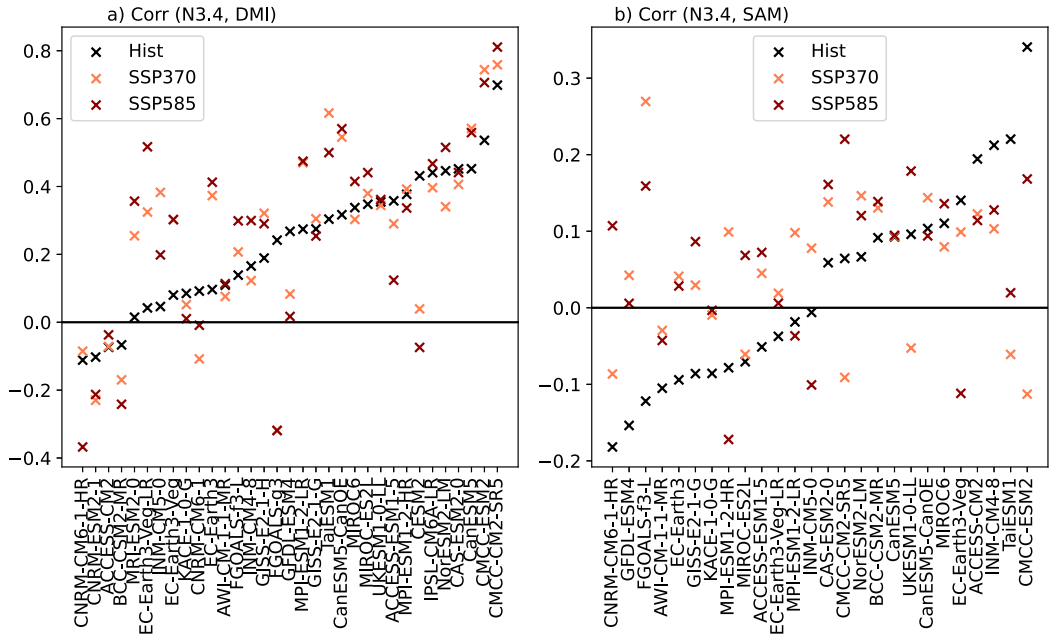

Figure 11. Correlations between (a) Nino3.4 and DMI, and (b) Nino3.4 and SAM for Historical (black), SSP370 (orange), and SSP585 (red) scenarios, using L20C and L21C periods. For context, observed correlations are r(Nino3.4,DMI) = 0.54 and r(Nino3.4,SAM) = −0.24 for 1980–2022.

Therefore while the percentage of models which project an increase in ENSO-IOD correlation or decrease in ENSO-SAM correlation are marginally higher than expected from internal variability, the degree of change largely lies within the range of internal variability. This indicates that projections of driver interactions due to external forcing are still uncertain, due to large inter-model spread, and possibly, multi-decadal variability.

5. Summary and Conclusions

In this study, we used 33 CMIP6 models and all available ensemble members to examine the change to DJF ENSO, SON IOD and SON SAM amplitude and frequency under SSP370 and SSP585 scenarios (between 1950–2014 and 2035–2099). We find that changes under SSP370 and SSP585 scenarios are similar, so will summarize here the overall projected changes.

We assess the statistical significance of change in two ways—first, we consider the change in the mean of the distributions of amplitude and frequency of events. Under this criterion, we find a significant increase in mean ENSO frequency, and a decrease in mean IOD amplitude. We also find a significant increase in mean SAM amplitude, and decrease in mean frequency of SAM events.

Second, we consider whether the forced changes in amplitude and frequency exceed that of the models' internal variability. We compare ΔAmplitude and ΔFrequency from the future scenarios to those generated by two 65-year periods in the piControl runs. Under this criteria, there are some differences in the responses of the driver phases. We find that for EN events, only <5% of total models (SSP370 and SSP585 combined) show a frequency or amplitude increase outside the 95% confidence interval obtained from the piControl changes. For LN events, a larger fraction of models project stronger, more frequent events, with 15% and 8% of models showing a degree of amplitude and frequency increase outside the piControl range, respectively. A previous study analysing ENSO amplitude changes in the ACCESS-ESM1.5 large ensemble also found that internal variability is large compared to the forced change (Rashid, 2022).

Compared to ENSO, a larger fraction of models project forced IOD and SAM changes outside the piControl range. Of the models, 25%–30% project a decrease in both pIOD and nIOD frequency. 35% of models project an amplitude decrease for pIOD events. However for nIOD, the results are more mixed, with 15% of models showing an amplitude increase, and 25% showing an amplitude decrease. Projections of SAM appear to be the most robust across models, with 50% of models exhibiting stronger events and 20% exhibiting less frequent events outside the

piControl range. We note that in the observed L20C period, there have been no significant observed trends in ENSO or IOD variability. However, the projected changes to SAM are consistent with a continuation of observed historical trends since the 1950s, that is, a strengthening of the SAM index (Marshall, 2003; Swart et al., 2015). Our findings are also consistent with previous studies which find a strengthening of SAM under high emissions scenarios (e.g., Deng et al., 2022). Although models generally project a future poleward shift in the Southern Hemisphere westerlies (i.e., a positive SAM trend), we note again that we are analysing here detrended values of all the indices as we are interested in the changes to the variability (amplitude and frequency) of the index.

We attempt to understand some of these driver changes through their relationship with mean state SST changes. We find that models with greater SST warming projection in the equatorial eastern Pacific also generally project a reduction in the amplitude of El Niño events. Similarly, the amount of warming projected in the Southern Ocean SSTs is inversely related to the change in El Niño amplitude across CMIP6 models. For La Niña events however the only region of mean state SST change of significance is a positive correlation between North Atlantic SSTs and the amplitude of La Niña events. In contrast, changes in IOD amplitude appear to be poorly related to mean state SST changes, while changes in SAM amplitude appear to scale with SST warming in general.

Our results are broadly consistent with previous ENSO and IOD-related studies using CMIP generation models. The increase in ENSO-driven SST variability has been identified in previous studies (e.g., Cai et al., 2022). New studies analysing extended model runs of 1000 years have also identified a decrease in IOD variability in response to increasing greenhouse gases, noting that a large degree of internal variability can mask this effect on centennial timescales (Kim et al., 2024; Wang, Cai, & Santoso, 2024). Interactions between the drivers and their impact on projections have been less studied, and projections of SAM are dependent on the sign of stratospheric ozone change. As ENSO and IOD events are highly covariant, it seems counterintuitive that the most likely pathways correspond to stronger and more frequent ENSO events, but weaker and less frequent IOD events. Experiments by Kim et al. (2024) suggest that while the degree of internal variability in the IOD is heavily influenced by the internal variability of ENSO, ENSO does not have a strong influence on the forced change of the IOD. Instead the authors suggest that the decrease in IOD amplitude is driven primarily by mean state changes in the Indian Ocean and associated feedback processes. Our results suggest that these processes may differ for pIOD and nIOD. While we have not separated moderate and strong pIOD events in this study, previous work has found a frequency decrease in moderate pIOD events but an increase in strong pIOD events (Cai et al., 2021; Wang, Cai, Santoso, et al., 2024). Further work can also shed light on processes in other models. This may include an assessment of ENSO-IOD coupling and its modulation by the Atlantic Multidecadal Oscillation (Xue et al., 2022), as well as an investigation into the known biases in the simulation of the IOD and how they impact the modeled relationship with ENSO.

Given the mixed responses of amplitude and frequency change amongst individual drivers, there is no clear indication of significant frequency change of concurrent driver phases. There remains a large spread amongst model runs, with only LN/neutral IOD/pSAM events showing a significant 35% frequency decrease under SSP585. Under SSP370, a significant 52% increase in LN/nIOD/nSAM events is found. Increases in LN-only and EN-only (with neutral IOD and SAM) are significant, with a 17%–18% increase in EN-only events projected under both scenarios, and a 13% increase in LN-only events under SSP370. It is worth noting that within the 65-year L20C period, there are generally few (<5) concurrent driver phases occurring in the Historical scenario. Therefore even mean changes on the order of 30%–50% correspond to increases or decreases of 0.5 events per 65-year.

In looking at changes to consecutive ENSO and IOD events, we find that although the MMEM shows a small increase in consecutive LN and pIOD events, and a decrease in consecutive nIOD events, the only statistically significant change is a 23% increase to pIOD events under SSP585. An earlier study which selected only 20 models (Geng et al., 2023) found a significant increase in consecutive LN, which highlights a key difference between the method employed in this study, and other evaluation-based studies.

As this study utilizes all available CMIP6 ensemble members, there are some caveats and points to note which we highlight here. There are known biases in the CMIP6 mean state and representation of the drivers which can impact these projections, such as some models having an overly biennial ENSO, or overly strong IOD (e.g., Mckenna et al., 2020). Another important point, as mentioned earlier, is the use of different model selection methods in obtaining projections. In using all available models and ensemble members, we sample the full range of internal and forced variability, weighting each model equally. Other approaches, such as model selection based

on certain criteria, may be better suited for projections based on specific physical processes (e.g., Delage & Power, 2020; Geng et al., 2023). For model selection for regional downscaling purposes, it may be desirable to select only a few models which sample a range of possible futures (e.g., Grose et al., 2023). Although such model selection may be necessary for practical or even scientific reasons, based on the results of the present study we suggest that if not carefully addressed, model selection may be unintentionally biased toward unrepresentative remote driver changes. We also note that selecting L21C events based on a future baseline is not the standard method used by most studies. However this is one method which takes into account that future events will not be defined based on historical baselines.

A further caveat of these findings is the choice of 0.75SD as a threshold for selecting events. While this threshold has been used in many previous studies (e.g., Eyring et al., 2021; Maher et al., 2023), we note that a lower threshold would identify more events while a higher threshold would identify fewer. In investigating the sensitivity of our results to lower or higher thresholds of 0.5SD and 1.0SD (not shown), we found that the changes to ΔAmplitude and ΔFrequency were generally consistent, however the statistical significance of the changes to ΔFrequency differed in some cases due to the different sample sizes.

While these results show that there is still a large amount of uncertainty in the projections of future driver changes, there are some interesting avenues for future work. Studies such as Rashid (2022) and Maher et al. (2023) showed that the forced ENSO amplitude change in large ensembles depends on zonal winds and the zonal SST gradient but can be complicated and non-linear. While the dynamics of forced changes in other models may vary, we show that there exists some relationship between the strengthening or weakening of drivers in a model and regional SST trends they project under high emission scenarios. Additionally, the projected changes to the relationship between drivers due to forced change is small in most models compared to internal variability. It is also worth noting that all CMIP6 models analysed here project an "El Nino-like" warming trend, which is in apparent contrast to the observed warming trend of the last few decades (Seager et al., 2019). While the reasons for this are the subject of ongoing research, it does lower confidence in projected changes in the tropical Pacific (Power et al., 2021). Our study shows that when considering future climate risk associated with remote drivers such as ENSO, IOD and SAM, a careful and representative consideration of both the forced changes of those drivers as well as plausible natural variations in the drivers and their combinations is necessary and is unlikely to be achieved with a limited sub-sample of models and experiments.

Data Availability Statement

All CMIP6 data used in this study is publicly available from https://esgf.nci.org.au/projects/esgf_nci/. Python scripts used for analysis are also publicly available from Chung and Boschat (2024).

Acknowledgments

The authors wish to thank the anonymous reviewers, Tim Cowan, Acacia Pepler, Andrea Taschetto, Doerte Jakob and David Jones for helpful reviews of this paper. This study was supported with funding from the Australian Government's National Environmental Science Program. Z.G. was supported by the ARC Centre of Excellence for Climate Extremes (CE170100023). This research was undertaken with the assistance of resources and services from the National Computational Infrastructure (NCI), which is supported by the Australian Government. We acknowledge the World Climate Research Programme, which, through its Working Group on Coupled Modeling, coordinated and promoted CMIP6. We thank the climate modeling groups for producing and making available their model output, the Earth System Grid Federation (ESGF) for archiving the data and providing access, and the multiple funding agencies who support CMIP6 and ESGF.

References

Behera, S. K., Luo, J.-J., & Yamagata, T. (2008). Unusual IOD event of 2007. *Geophysical Research Letters*, *35*(14), L14S11. https://doi.org/10.1029/2008GL034122

Cai, W., Cowan, T., & Raupach, M. (2009). Positive Indian Ocean Dipole events precondition southeast Australia bushfires. *Geophysical Research Letters*, *36*(19), L19710. https://doi.org/10.1029/2009GL039902

Cai, W., Ng, B., Wang, G., Santoso, A., Wu, L., & Yang, K. (2022). Increased ENSO sea surface temperature variability under four IPCC emission scenarios. *Nature Climate Change*, *12*(3), 228–231. https://doi.org/10.1038/s41558-022-01282-z

Cai, W., Pan, A., Roemmich, D., Cowan, T., & Guo, X. (2009). Argo profiles a rare occurrence of three consecutive positive Indian Ocean Dipole events, 2006–2008. *Geophysical Research Letters*, *36*(8), L08701. https://doi.org/10.1029/2008GL037038

Cai, W., Yang, K., Wu, L., Huang, G., Santoso, A., Ng, B., et al. (2021). Opposite response of strong and moderate positive Indian Ocean Dipole to global warming. *Nature Climate Change*, *11*(1), 27–32. https://doi.org/10.1038/s41558-020-00943-1

Chung, C. T. Y., & Boschat, G. (2024). CMIP6 driver pathways scripts. *Zenodo*. https://doi.org/10.5281/zenodo.13788228

Chung, C. T. Y., Boschat, G., Taschetto, A., Narsey, S., McGregor, S., Santoso, A., & Delage, F. (2023). Evaluation of seasonal teleconnections to remote drivers of Australian rainfall in CMIP5 and CMIP6 models. *Journal of Southern Hemisphere Earth Systems Science*, *73*(3), 219–261. https://doi.org/10.1071/es23002

Delage, F. P. D., & Power, S. B. (2020). The impact of global warming and the El Niño-Southern Oscillation on seasonal precipitation extremes in Australia. *Climate Dynamics*, *54*(9–10), 4367–4377. https://doi.org/10.1007/s00382-020-05235-0

Deng, K., Azorin-Molina, C., Yang, S., Hu, C., Zhang, G., Minola, L., & Chen, D. (2022). Changes of Southern Hemisphere westerlies in the future warming climate. *Atmospheric Research*, *270*, 106040. https://doi.org/10.1016/j.atmosres.2022.106040

Eyring, V., Bony, S., Meehl, G. A., Senior, C. A., Stevens, B., Stouffer, R. J., & Taylor, K. E. (2016). Overview of the coupled model intercomparison project phase 6 (CMIP6) experimental design and organization. *Geoscientific Model Development*, *9*(5), 1937–1958. https://doi.org/10.5194/gmd-9-1937-2016

Eyring, V., Gillett, N. P., Achuta Rao, K. M., Barimalala, R., Barreiro Parrillo, M., Bellouin, N., et al. (2021). Human Influence on the Climate System. In V. Masson-Delmotte, P. Zhai, A. Pirani, S. L. Connors, C. Péan, S. Berger, et al. (Eds.) *Climate Change 2021: The Physical Science*

Basis. Contribution of Working Group I to the Sixth Assessment Report of the Intergovernmental Panel on Climate Change (pp. 423–552). Cambridge University Press. https://doi.org/10.1017/9781009157896.005

Geng, T., Jia, F., Cai, W., Wu, L., Gan, B., Jing, Z., et al. (2023). Increased occurrences of consecutive La Niña events under global warming. *Nature*, *619*(7971), 774–781. https://doi.org/10.1038/s41586-023-06236-9

Gillett, Z. E., Taschetto, A. S., Holgate, C. M., & Santoso, A. (2023). Linking ENSO to synoptic weather systems in eastern Australia. *Geophysical Research Letters*, *50*(15), e2023GL104814. https://doi.org/10.1029/2023GL104814

Gong, D., & Wang, S. (1999). Definition of Antarctic oscillation index. *Geophysical Research Letters*, *26*(3), 459–462. https://doi.org/10.1029/1999gl900003

Goyal, R., Sen Gupta, A., Jucker, M., & England, M. H. (2021). Historical and projected changes in the Southern Hemisphere surface westerlies. *Geophysical Research Letters*, *48*(4), e2020GL090849. https://doi.org/10.1029/2020GL090849

Grose, M. R., Narsey, S., Delage, F. P., Dowdy, A. J., Bador, M., Boschat, G., et al. (2020). Insights from CMIP6 for Australia's future climate. *Earth's Future*, *8*(5), e2019EF001469. https://doi.org/10.1029/2019EF001469

Grose, M. R., Narsey, S., Trancoso, R., Mackallah, C., Delage, F., Dowdy, A., et al. (2023). A CMIP6-based multi-model downscaling ensemble to underpin climate change services in Australia. *Climate Services*, *30*, 100368. https://doi.org/10.1016/j.cliser.2023.100368

Hendon, H. H., Thompson, D. W. J., & Wheeler, M. C. (2007). Australian rainfall and surface temperature variations associated with the Southern Hemisphere annular mode. *Journal of Climate*, *20*(11), 2452–2467. https://doi.org/10.1175/JCLI4134.1

Hu, X., Eichner, J., Gong, D., Barreiro, M., & Kantz, H. (2023). Combined impact of ENSO and Antarctic Oscillation on austral spring precipitation in Southeastern South America (SESA). *Climate Dynamics*, *61*(1–2), 399–412. https://doi.org/10.1007/s00382-022-06592-8

Huang, A. T., Gillett, Z. E., & Taschetto, A. S. (2024). Australian rainfall increases during multi-year La Niña. *Geophysical Research Letters*, *51*(9), e2023GL106939. https://doi.org/10.1029/2023gl106939

Hui, C., & Zheng, X. T. (2018). Uncertainty in Indian Ocean Dipole response to global warming: The role of internal variability. *Climate Dynamics*, *51*(9–10), 3597–3611. https://doi.org/10.1007/s00382-018-4098-2

Jeong, H., Park, H., Chowdary, J., & Xie, S. (2023). Triple-Dip La Niña contributes to Pakistan flooding and southern China drought in summer 2022. *Bulletin of the American Meteorological Society*, *104*(9), E1570–E1586. https://doi.org/10.1175/bams-d-23-0002.1

Kim, S. K., Park, H. J., An, S. I., Liu, C., Cai, W., Santoso, A., & Kug, J. S. (2024). Decreased Indian Ocean Dipole variability under prolonged greenhouse warming. *Nature Communications*, *15*(1), 2811. https://doi.org/10.1038/s41467-024-47276-7

Liguori, G., McGregor, S., Singh, M., Arblaster, J., & Di Lorenzo, E. (2022). Revisiting ENSO and IOD contributions to Australian precipitation. *Geophysical Research Letters*, *49*(1), e2021GL094295. https://doi.org/10.1029/2021GL094295

Lim, E.-P., Hendon, H. H., Arblaster, J. M., Delage, F., Nguyen, H., Min, S.-K., & Wheeler, M. C. (2016). The impact of the Southern Annular Mode on future changes in Southern Hemisphere rainfall. *Geophysical Research Letters*, *43*(13), 7160–7167. https://doi.org/10.1002/2016GL069453

Lin, J., & Qian, T. (2019). A new picture of the global impacts of El Nino-Southern Oscillation. *Scientific Reports*, *9*(1), 17543. https://doi.org/10.1038/s41598-019-54090-5

Maher, N., Wills, R. C. J., DiNezio, P., Klavans, J., Milinski, S., Sanchez, S. C., et al. (2023). The future of the El Niño–Southern Oscillation: Using large ensembles to illuminate time-varying responses and inter-model differences. *Earth System Dynamics*, *14*(2), 413–431. https://doi.org/10.5194/esd-14-413-2023

Marshall, G. J. (2003). Trends in the southern annular mode from observations and reanalyses. *Journal of Climate*, *16*(24), 4134–4143. https://doi.org/10.1175/1520-0442(2003)016<4134:TITSAM>2.0.CO;2

McKay, D. I. A., Staal, A., Abrams, J. F., Winkelmann, R., Sakschewski, B., Loriani, S., et al. (2022). Exceeding 1.5°C global warming could trigger multiple climate tipping points. *Science*, *377*(6611), eabn7950. https://doi.org/10.1126/science.abn7950

McKay, R. C., Boschat, G., Rudeva, I., Pepler, A., Purich, A., Dowdy, A., et al. (2023). Can southern Australian rainfall decline be explained? A review of possible drivers. *WIREs Climate Change*, *14*(2), e820. https://doi.org/10.1002/wcc.820

McKenna, S., Santoso, A., Gupta, A. S., Taschetto, A. S., & Cai, W. (2020). Indian Ocean Dipole in CMIP5 and CMIP6: Characteristics, biases, and links to ENSO. *Scientific Reports*, *10*(1), 11500. https://doi.org/10.1038/s41598-020-68268-9

McPhaden, M. J., Santoso, A., & Cai, W. (2020). Introduction to El Niño Southern Oscillation in a changing climate. In M. J. McPhaden, A. Santoso, & W. Cai (Eds.), *El Niño Southern Oscillation in a changing climate*. https://doi.org/10.1002/9781119548164.ch1

Meinshausen, M., Nicholls, Z. R. J., Lewis, J., Gidden, M. J., Vogel, E., Freund, M., et al. (2020). The shared socio-economic pathway (SSP) greenhouse gas concentrations and their extensions to 2500. *Geoscientific Model Development*, *13*(8), 3571–3605. https://doi.org/10.5194/gmd-13-3571-2020

Okumura, Y. M., DiNezio, P., & Deser, C. (2017). Evolving impacts of multiyear La Niña events on atmospheric circulation and U.S. drought. *Geophysical Research Letters*, *44*(22), 11614–11623. https://doi.org/10.1002/2017GL075034

Power, S. B., & Delage, F. P. D. (2018). El Niño–Southern Oscillation and associated climatic conditions around the world during the latter half of the twenty-first century. *Journal of Climate*, *31*(15), 6189–6207. https://doi.org/10.1175/JCLI-D-18-0138.1

Power, S. B., Lengaigne, M., Capotondi, A., Khodri, M., Vialard, J., Jebri, B., et al. (2021). A review of decadal climate variability in the tropical Pacific: Characteristics, causes, predictability and prospects. *Science*, *374*(6563). https://doi.org/10.1126/science/aay9165

Rashid, H. A. (2022). Forced changes in El Niño–Southern Oscillation due to global warming and the associated uncertainties in ACCESS-ESM1.5 large ensembles. *Frontiers in Climate*, *4*, 954449. https://doi.org/10.3389/fclim.2022.954449

Reddy, P. J., Perkins-Kirkpatrick, S. E., Ridder, N. N., & Sharples, J. J. (2022). Combined role of ENSO and IOD on compound drought and heatwaves in Australia using two CMIP6 large ensembles. *Weather and Climate Extremes*, *37*, 100469. https://doi.org/10.1016/j.wace.2022.100469

Riahi, K., van Vuuren, D. P., Kriegler, E., Edmonds, J., O'Neill, B. C., Fujimori, S., et al. (2017). The Shared Socioeconomic Pathways and their energy, land use, and greenhouse gas emissions implications: An overview. *Global Environmental Change*, *42*, 153–168. https://doi.org/10.1016/j.gloenvcha.2016.05.009

Risbey, J. S., Pook, M. J., McIntosh, P. C., Wheeler, M. C., & Hendon, H. H. (2009). On the remote drivers of rainfall variability in Australia. *Monthly Weather Review*, *137*(10), 3233–3253. https://doi.org/10.1175/2009MWR2861.1

Saji, N., Goswami, B., Vinayachandran, P., & Yamagata, T. (1999). A dipole mode in the tropical Indian Ocean. *Nature*, *401*(6751), 360–363. https://doi.org/10.1038/43854

Saji, N., & Yamagata, T. (2003). Possible impacts of Indian Ocean Dipole mode events on global climate. *Climate Research*, *25*(2), 151–169. https://doi.org/10.3354/cr025151

Seager, R., Cane, M., Henderson, N., Lee, D. E., Abernathey, R., & Zhang, H. (2019). Strengthening tropical Pacific zonal sea surface temperature gradient consistent with rising greenhouse gases. *Nature Climate Change*, *9*(7), 517–522. https://doi.org/10.1038/s41558-019-0505-x

Shiogama, H., Fujimori, S., Hasegawa, T., Hayashi, M., Hirabayashi, Y., Ogura, T., et al. (2023). Important distinctiveness of SSP3–7.0 for use in impact assessments. *Nature Climate Change*, *13*(12), 1276–1278. https://doi.org/10.1038/s41558-023-01883-2

Silvestri, G. E., & Vera, C. S. (2003). Antarctic Oscillation signal on precipitation anomalies over southeastern South America. *Geophysical Research Letters*, *30*(21), 2155. https://doi.org/10.1029/2003GL018277

Swart, N. C., Fyfe, J. C., Gillett, N., & Marshall, G. J. (2015). Comparing trends in the southern annular mode and surface westerly jet. *Journal of Climate*, *28*(22), 8840–8859. https://doi.org/10.1175/jcli-d-15-0334.1

Trenberth, K. E. (1979). Interannual variability of the 500 mb zonal flow in the Southern Hemisphere. *Monthly Weather Review*, *107*(11), 1515–1524. https://doi.org/10.1175/1520-0493(1979)107<1515:ivotmz>2.0.co;2

Wang, G., & Cai, W. (2020). Two-year consecutive concurrences of positive Indian Ocean Dipole and Central Pacific El Niño preconditioned the 2019/2020 Australian "black summer" bushfires. *Geoscience Letters*, *7*(1), 19. https://doi.org/10.1186/s40562-020-00168-2

Wang, G., Cai, W., & Santoso, A. (2024). Variability of the Indian Ocean Dipole post-2100 reverses to a reduction despite persistent global warming. *Nature Communications*, *15*(1), 5023. https://doi.org/10.1038/s41467-024-49401-y

Wang, G., Cai, W., Santoso, A., Abram, N., Ng, B., Yang, K., et al. (2024). The Indian Ocean Dipole in a warming world. *Nature Reviews Earth & Environment*, *5*(8), 588–604. https://doi.org/10.1038/s43017-024-00573-7

Xue, J., Luo, J.-J., Zhang, W., & Yamagata, T. (2022). ENSO–IOD inter-basin connection is controlled by the Atlantic Multidecadal Oscillation. *Geophysical Research Letters*, *49*(24), e2022GL101571. https://doi.org/10.1029/2022GL101571

Yin, H., Fowler, H. J., Blenkinsop, S., Wu, Z., He, H., & Li, Y. (2023). ENSO and IOD contributions to seasonal meteorological droughts over the Yangtze River basin. *International Journal of Climatology*, *43*(16), 8120–8136. https://doi.org/10.1002/joc.8311

Yin, H., Wu, Z., Fowler, H. J., Blenkinsop, S., He, H., & Li, Y. (2022). The combined impacts of ENSO and IOD on global seasonal droughts. *Atmosphere*, *13*(10), 1673. https://doi.org/10.3390/atmos13101673

Yu, B., Zhang, X., Lin, H., & Yu, J.-Y. (2015). Comparison of wintertime North American climate impacts associated with multiple ENSO indices. *Atmosphere-Ocean*, *53*(4), 426–445. https://doi.org/10.1080/07055900.2015.1079697

Zheng, F. (2023). Slowing down of the summer Southern Hemisphere Annular Mode trend against the background of ozone recovery. *Atmospheric and Oceanic Science Letters*, *17*(1), 100375. https://doi.org/10.1016/j.aosl.2023.100375

Erratum

The originally published version of this article contained a typographical error. Figures 3 and 5 were identical. The error has been corrected, and this may be considered the authoritative version of record.